Application of Blind Deconvolution Denoising in Failure Prognosis

Bin Zhang, *Senior Member, IEEE*, Taimoor Khawaja, Romano Patrick, George Vachtsevanos, *Senior Member, IEEE*, Marcos E. Orchard, and Abhinav Saxena, *Member, IEEE*

***Abstract*—Fault diagnosis and failure prognosis are essential techniques in improving the safety of many mechanical systems. However, vibration signals are often corrupted by noise; therefore, the performance of diagnostic and prognostic algorithms is degraded. In this paper, a novel denoising structure is proposed and applied to vibration signals collected from a testbed of the helicopter main gearbox subjected to a seeded fault. The proposed structure integrates a denoising algorithm, feature extraction, failure prognosis, and vibration modeling into a synergistic system. Performance indexes associated with the quality of the extracted features and failure prognosis are addressed, before and after denoising, for validation purposes.**

***Index Terms*—Blind deconvolution, decision support system, deconvolution, denoising, failure prognosis, fault diagnosis, gearbox vibration signal, signal processing.**

I. Introduction

THE performance of failure prognostic algorithms is closely related to features (also known as condition indicators) derived from sensor data, which reveal the evolution and propagation of a failure in the system [1]–[3]. For many mechanical systems, features are typically extracted from vibration data [4]. Noise, however, often corrupts the vibration signals and masks the indication of faults, particularly in their early stages, thus curtailing the ability to accurately diagnose and predict failures. Therefore, it is important to develop a good denoising scheme for improving the signal-to-noise ratio (SNR) and making the characteristics of the fault perceptible in the vibration data. This process will improve the quality of the features, potentially lower the fault-detection threshold, and thus increase the accuracy of the diagnostic and prognostic algorithms.

The main transmission of Blackhawk and Seahawk helicopters employs an epicyclic gear system [4], [5]. Recently, a crack in the planetary carrier plate was discovered and resulted in a major overhaul and replacement of gear plates at a high cost. Therefore, many research efforts toward designing and implementing condition-based maintenance (CBM) on helicopters, such as signal preprocessing [2], [6], vibration signal modeling [7], feature extraction [2], [3], detection of cracks, and prediction of crack length [8], [13], have been carried out. The objective of this paper is to propose a new vibration preprocessing structure, which synergizes vibration denoising, vibration modeling, feature extraction, and failure prognosis, to enhance the performance of CBM. The planetary gear system with a seeded crack on the gear carrier plate will be used to verify the proposed method.

For an epicyclic gear system, the widely used denoising technique is time synchronous averaging (TSA), which can be implemented in the time or frequency domain [2]–[4]. Other denoising algorithms include blind source separation [9], stochastic resonance [10], and adaptive schemes [11]. Since previous research [7] has provided a good understanding of the true vibration signals, a blind deconvolution algorithm developed for a similarly formulated image processing problem [12] will be modified and employed to recover the actual vibration signal [14]. This paper addresses in detail the structure of the overall denoising scheme, the analysis of vibration mechanisms, the blind deconvolution algorithm, and its experimental verification. The results show that the proposed denoising scheme can substantially improve the SNR, feature performance, and the precision of the failure prognostic algorithm. The developed algorithm has successfully been applied to real-time fault diagnosis and failure prognosis [15].

II. Denoising Scheme Architecture

The proposed denoising scheme is shown in Fig. 1. An accelerometer mounted on the gearbox frame collects vibration signals, which, in turn, are preprocessed to obtain TSA signal $s(t)$. The blind deconvolution denoising algorithm is carried out in the frequency domain. Thus, the denoising algorithm is applied to $S(f)$, which outputs the denoised vibration data in the frequency domain $B(f)$. If the time-domain signal is required, $B(f)$ can be inverse Fourier transformed to obtain $b(t)$.

Manuscript received October 30, 2007; revised April 22, 2008. First published October 28, 2008; current version published January 5, 2009. This work was supported in part by the Defense Advanced Research Projects Agency Structural Integrity Prognosis Program (SIPS) under the direction of Dr. L. Christodoulou. The Associate Editor coordinating the review process for this paper was Dr. John Sheppard.

B. Zhang and T. Khawaja are with the School of Electrical and Computer Engineering, Georgia Institute of Technology, Atlanta, GA 30332 USA (e-mail: bin.zhang@gatech.edu).

R. Patrick is with Impact Technologies, LLC, Rochester, NY 14623 USA (e-mail: romano.patrick@impact-tek.com).

G. Vachtsevanos is with the Georgia Institute of Technology, Atlanta, GA 30332 USA, and also with Impact Technologies, LLC, Rochester, NY 14623 USA (e-mail: gjv@ece.gatech.edu).

M. Orchard is with the Department of Electrical Engineering, University of Chile, Santiago 837-0451, Chile (e-mail: morchard@ing.uchile.cl).

A. Saxena is with Research Institute for Advanced Computer Science, Prognostics Center of Excellence, NASA Ames Research Center, Moffett Field, CA 94035 USA (e-mail: abhinav.saxena@nasa.gov).

Color versions of one or more of the figures in this paper are available online at http://ieeexplore.ieee.org.

Digital Object Identifier 10.1109/TIM.2008.2005963

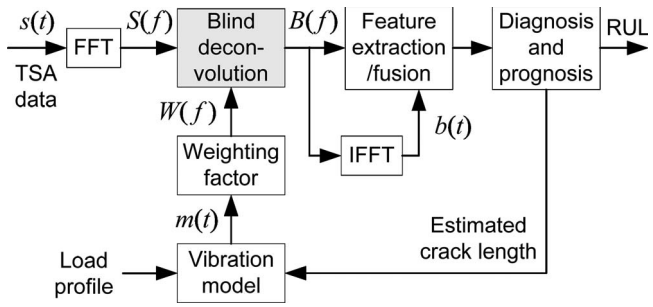

Fig. 1. Overall structure of the denoising scheme.

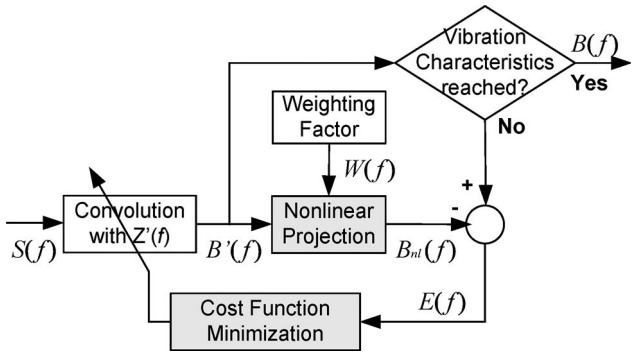

Fig. 2. Blind deconvolution denoising scheme.

From $B(f)$ and $b(t)$, features can be extracted and fused to subsequently be used in fault-diagnostic and failure-prognostic routines. The failure-prognostic algorithm not only predicts the remaining useful life (RUL) of the system but also provides an estimate of the crack length on the planet gear carrier plate as a function of time [8], [13]. Both the estimated crack length and load profile of the helicopter serve as inputs to the vibration model [7], which generates the modeled vibration signal $m(t)$. The frequency spectra of $m(t)$ are normalized to obtain weighting factor vector $W(f)$, which is used in a nonlinear projection of the algorithm.

The blind deconvolution algorithm is shown in Fig. 2. The nonlinear projection, which is based on vibration analysis in the frequency domain, and the cost function minimization blocks are critical components. Initially, an inverse filter $Z'(f)$ must be defined. This filter is an initial estimate of the inverse modulating signal in the frequency domain and converges to a filter, through an optimization algorithm, that recovers the vibration signal from the noisy measured data $S(f)$. Inverse filter $Z'(f)$ is convoluted with $S(f)$ to obtain a rough estimate of vibration signal $B'(f)$. Signal $B'(f)$ passes through the nonlinear projection, which maps $B'(f)$ to a subspace that contains only known characteristics of the vibration signal, to yield $B_{\rm nl}(f)$. The difference between $B'(f)$ and $B_{\rm nl}(f)$ is denoted as $E(f)$. By iteratively adjusting $Z'(f)$ to minimize $E(f)$ and when the difference of $E(f)$ in two successive iterations reach a threshold value or, in the real-time case, the iteration number reaches a given value, it can be said that signal $B'(f)$ approaches $B(f)$, which can be regarded as the denoised vibration signal. At the same time, $Z'(f)$ approaches $Z(f)$, which is close enough to a real inverse filter.

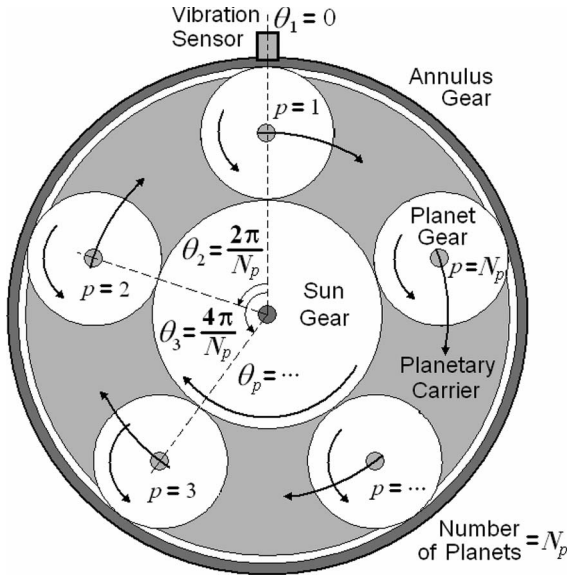

Fig. 3. Configuration of an epicyclic gear system.

III. Vibration Data Analysis

The vibration signals are derived from a main transmission gearbox with five planet gears, as shown in Fig. 3. The gearbox has a seeded crack fault on the planetary gear plate. The succeeding sections intend to describe the expected vibration data.

A. Healthy Gearbox

Ideally, planetary gears are evenly spaced. The accelerometer is mounted at a fixed point at position $\theta = 0$. Then, the modulating signal for planetary gear p has the form

$$a_p(t) = \sum_{n=-N}^{N} \alpha_n \cos(n\theta_p) \tag{1}$$

where θ_p is the position of gear p, f^s is the carrier rotation frequency, N is the number of sidebands under consideration, and α_n is the amplitude of the frequency component at frequency nf^s.

Mesh vibrations generated from different gears are of the same amplitude but different phase shifts. Since the teeth meshing speed is proportional to the angular velocity of the planetary carrier, the meshing vibration appears at frequencies $N_t f^s$ [5], [7], with N_t being the number of annulus gear teeth. Then, the vibration signal from gear p can be written as

$$b_p(t) = \sum_{m=1}^{M} \beta_m \sin(mN_t\theta_p) \tag{2}$$

where M is the number of harmonics under consideration, and β_m is the harmonic amplitude of the meshing vibration.

Then, the observed vibration signal of planetary gear p, with respect to the static accelerometer, is given as the product of the meshing vibration signal and the amplitude-modulating

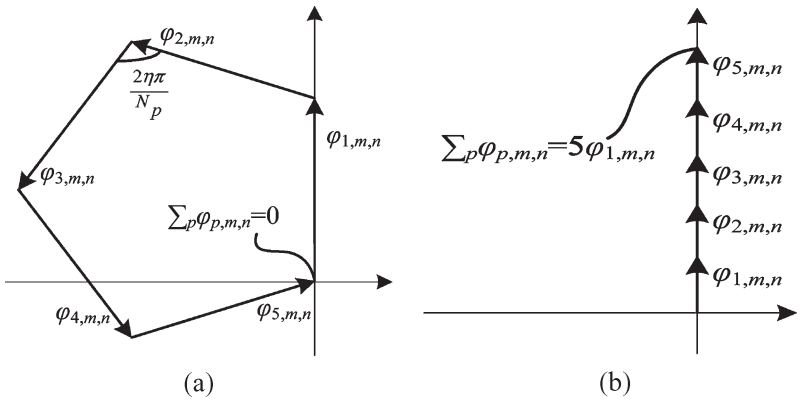

Fig. 4. Superposition for a faulty gear plate. (a) $mN_t + n \neq kN_p$ (non-RMC). (b) $mN_t + n = kN_p$ (RMC).

signal. This signal, which is denoted by $y_p(t) = a_p(t)b_p(t)$, is given by

$$y_p(t) = \frac{1}{2}\sum_{m=1}^{M}\sum_{n=-N}^{N}\alpha_n\beta_m \sin(mN_t + n)\theta_p). \tag{3}$$

The position of the frequency components around the meshing vibration harmonics (or sidebands) are located at $(mN_t + n)f^s$.

When there are N_p planetary gears, the vibration signal observed by the accelerometer is the superposition of the vibration signals generated from N_p different planetary gears. This superposed vibration signal has the form

$$y(t) = \frac{1}{2}\sum_{p=1}^{N_p}\sum_{m=1}^{M}\sum_{n=-N}^{N}\alpha_n\beta_m \sin\left(2\pi(p-1)\frac{mN_t + n}{N_p}\right). \tag{4}$$

Since the planetary gears are evenly spaced, the phase angle of the sidebands will be evenly spaced along 2π [5]. Thus, it is obvious that, if sideband $mN_t + n$ is not a multiple of N_p and $(mN_t + n)/N_p$ has a remainder of γ, the vibration components from different gears are evenly spaced by an angle $2\gamma\pi/N_p$. In this case, when the vibrations generated from different planetary gears are combined, these sidebands add destructively and become zero. Those frequency components appear at sidebands where $mN_t + n \neq kN_p$ are termed as nonregular meshing components (non-RMC). This case is shown in Fig. 4(a).

On the contrary, if sideband $mN_t + n$ is a multiple of N_p, the remainder of $(mN_t + n)/N_p$ will be zero. In this case, the vibration components from different gears do not have a phase difference. When the vibration signals from different planetary gears are combined, these sidebands add constructively and are reinforced. These frequency components that appear at sidebands where $mN_t + n = kN_p$ are referred to as regular meshing components (RMCs) or apparent sidebands. This process of frequency components adding destructively/constructively finally generates asymmetrical sidebands [5], [7]. This case is shown in Fig. 4(b).

According to the aforementioned vibration analysis in the frequency domain as well as from previous research results for an ideal system [4], [5], [7], only the spectra at frequencies that are multiples of the number of planetary gears (i.e., RMC) survive, whereas the spectra at other frequencies (i.e., non-RMC) vanish. With this understanding, the vibration data in the frequency domain can be written as

$$Y(f) = f_{\text{hea}}\left(\gamma_{m,n}\left((mN_t + n)f^s\right)\right) \tag{5}$$

where $\gamma_{m,n}$ is the magnitude of the spectral amplitude at $(mN_t + n)f^s$, and f_{hea} is the nonlinear projection for an ideal healthy gearbox given by

$$f_{\text{hea}} = \begin{cases} 1, & \text{if } mN_t + n \text{ is a multiple of } N_p \\ 0, & \text{otherwise.} \end{cases} \tag{6}$$

B. Faulty Gearbox

When the planetary gear carrier has a crack, the gears are no longer being evenly separated along 2π. For analysis simplicity, suppose that only one planetary gear has an angle shift. Due to this phase shift, when $mN_t + n$ is not a multiple of N_p, the vibration components from different gears will not be canceled in destructive adding, as shown in Fig. 5(a), where $\varphi_{p,m,n}$, with $1 \leq p, \leq 5$ indicates the frequency components of gear p at frequency $(mN_t + n)f^s$. This results in higher non-RMC frequency components.

On the other hand, when $mN_t + n$ is a multiple of N_p, the vibration components from different gears are not exactly in phase, which results in lower RMC frequency components, as shown in Fig. 5(b).

Therefore, the nonlinear projection for a healthy gearbox is not suitable for a faulty gearbox. A modification of the nonlinear projection is given as follows: From previous research in [7], a vibration model in the frequency domain has been established, with the load profile and the crack size being two of the inputs. Note that the load profile is known and that the crack size can be estimated from the prognostic algorithm [8], [13]. Then, the modeled noise-free vibration signal $m(t)$ generated from the vibration model is Fourier transformed in the frequency domain to arrive at $M(f)$. The magnitude of $M(f)$ is normalized to obtain weighting factors $W(f)$.

When a frequency-domain signal $B'(f)$ is fed into the nonlinear projection, it yields $B_{\text{nl}}(f)$. Supposing that $\lambda_{m,n}$ is the

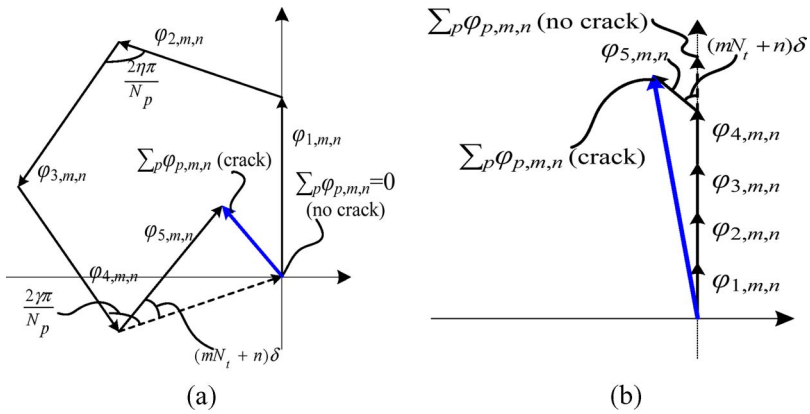

Fig. 5. Superposition for a faulty gear plate. (a) $mN_t + n \neq kN_p$ (non-RMC). (b) $mN_t + n = kN_p$ (RMC).

magnitude of the sideband at $(mN_t + n)f^s$, the spectra of $B'(f)$ can be written as $\lambda_{m,n}((mN_t + n)f^s)$, and accordingly, the spectra of $B_{\rm nl}(f)$ are given by $W_{m,n}(f)\lambda_{m,n}((mN_t + n)f^s)$, where $W_{m,n}(f)$ is the weighting factor at sideband $mN_t + n$ defined by $W(f)$. It is clear that the nonlinear projection in this case is

$$f_{\rm nl} = W_{m,n}(f) \qquad \forall (mN_t + n) \in D_{\rm sup}. \tag{7}$$

Note that $f_{\rm hea}$ is a special case of $f_{\rm nl}$.

IV. Blind Deconvolution Denoising

From the vibration analysis of the gearbox, we know that the vibration signals collected from the transducer are amplitude modulated [5], [7]. Multiple sources of noise may further corrupt the signal. A simplified model for such a complex signal may be defined as

$$s(t) = a(t)b(t) + n(t) \tag{8}$$

where $s(t)$ is the measured vibration signal, $b(t)$ is the noise-free unmodulated vibration signal, $a(t)$ is the modulating signal, and $n(t)$ is the cumulative additive noise.

Previous research results detail the spectral characteristics of vibration signals for rotating equipment [6], [7], [9]. It is appropriate, therefore, to investigate the measured noisy vibration in the frequency domain. Thus, the model can be written in the frequency domain as

$$S(f) = A(f) * B(f) + N(f) \tag{9}$$

where $*$ is the convolution operator, and $S(f)$, $A(f)$, $B(f)$, and $N(f)$ are the Fourier transforms of $s(t)$, $a(t)$, $b(t)$, and $n(t)$, respectively. Then, the goal in the frequency domain is to recover $B(f)$.

To solve this problem, we start with $Z'(f)$, a very rough initial estimate of the inverse filter, which demodulates the observed signal $S(f)$ to give a rough noise-free vibration signal

$$B'(f) = S(f) * Z'(f). \tag{10}$$

Passing $B'(f)$ through the nonlinear projection, it yields $B_{\rm nl}(f)$. The difference between $B_{\rm nl}(f)$ and $B'(f)$, which is denoted as $E(f)$, is minimized afterward. The iterative process refines $Z'(f)$ to minimize $E(f)$. When the difference in $E(f)$ in two successive iterations reach a threshold value, $Z'(f)$ converges to $Z(f)$, which is close enough to a real inverse filter. Then, with this $Z(f)$, a good estimate for $B(f)$ is obtained as

$$B(f) = S(f) * Z(f). \tag{11}$$

Two additional assumptions are made in the solution of this problem.

1) $Z(f)$ exists and is summable, i.e., $\sum Z(f) < \infty$.
2) Since the modulating signal $a(t)$ is always positive, its inverse is also positive.

The cost function for the optimization is defined as

$$J = \sum_{f \in D_{\rm sup}} \left[B'(f) - B_{\rm nl}(f)\right]^2 + \left(\sum Z(f) - 1\right)^2 \tag{12}$$

where $D_{\rm sup}$ is the frequency range that contains the main vibration information. Because of the periodic fade of signal spectra between harmonics, a window centered at harmonic frequencies is used to define critical frequencies. All these windows, for a certain number of harmonics, form the support $D_{\rm sup}$. In the cost function, assumptions 1 and 2 are used to arrive at the second term to avoid an all-zero inverse filter $Z(f)$, which leads to the trivial solution for error minimization. Moreover, the iterative conjugate gradient method is called upon to address the optimization problem. This method has a faster convergence rate in general, as compared with the steepest descent method [12].

V. Experimental Studies

This section presents some experimental results from a helicopter gearbox that has a plate with seeded fault. To highlight the effectiveness of the proposed blind deconvolution denoising method, it is compared with a spectral subtraction denoising method [16]. The comparison is between the SNR and performance of the extracted feature.

A. Data and Feature

The initial length of the seeded crack on the carrier is 1.344 in and grows with the evolving operation of the gearbox. The gearbox operates over a large number of ground–air–ground (GAG) cycles at different torque levels. In each GAG cycle the torque increases from 20% to 40%, then to 100%, and, finally, to 120%; it then decreases to 20% for the next cycle. Each GAG cycle is about 3 min.

In each GAG cycle, the torque levels at 20%, 40%, and 100% are investigated. This way, vibration data are acquired at different torque levels and different crack lengths. Analysis in Section III shows that the ratio of the non-RMC to the RMC sidebands may indicate the presence of a fault on the planetary carrier. Based on this notion, the feature sideband ratio (SBR) [2] will be used to demonstrate the effectiveness of the denoising algorithm. Let X denote the number of sidebands in consideration on both sides of the dominant harmonic components; SBR is then defined as

$$\mathrm{SBR}(X) = \frac{\sum_{h=1}^{m}\sum_{g=-X}^{X}\text{non-RMC}}{\sum_{h=1}^{m}\sum_{g=-X}^{X}(\text{non-RMC}+\text{RMC})}. \tag{13}$$

B. Performance on Signal and Feature

The first performance index is an overall accuracy measure defined as the linear correlation coefficient between the raw feature values and the crack length growth (CCR) [7]. In the experiment, the ground truth crack length data at discrete GAG cycles are available. With these data, the crack growth curve can be obtained through interpolation. Suppose that x is the feature vector and that y is the crack growth curve, with $\underline{x}$ and $\underline{y}$ being their means, respectively. The correlation coefficient between x and y is given as

$$\mathrm{CCR}(x,y) = \sqrt{\frac{ss_{xy}^2}{ss_{xx}ss_{yy}}} \tag{14}$$

where $ss_{xy}=\sum_{i=1}^{l_x}(x_i-\underline{x}_i)(y_i-\underline{y}_i)$, $ss_{xx}=\sum_{i=1}^{l_x}(x_i-\underline{x}_i)^2$, and $ss_{yy}=\sum_{i=1}^{l_x}(y_i-\underline{y}_i)^2$, respectively, and l_x is the length of feature vector x.

Because of the changes in operating conditions and other disturbances, the feature values along the GAG axis are very noisy and need to be smoothed through a low-pass filtering operation. Then, an accuracy performance index is obtained by calculating the correlation coefficient based on the smoothed feature curve x' (CCS) [7]. The calculation of CCS is the same as that of CCR in (14), except that x is being replaced by x'. To obtain x', a Butterworth low-pass filter with a cutoff frequency of 0.2π is used.

The third performance index is a precision measure corresponding to a normalized measure of the signal dispersion. It is referred to as percent mean deviation (PMD) [7], i.e.,

$$\mathrm{PMD}(x,\tilde{x}) = \frac{\sum_{i=1}^{l_x}\frac{x_i-x_i'}{x_i'}}{l_x}\times 100. \tag{15}$$

The SNRs, before and after denoising, at 100% torque levels are shown in Fig. 6(a). It is clear that the signal after the blind deconvolution denoising routine enjoys the highest SNR, which is desirable. The feature of SBR(12) at 100% torque level is shown in Fig. 6(b). The correlation coefficient and PMD for this feature at different torque levels are summarized in Table I. At the 100% torque level, the CCR, CCS, and PMD of the feature from the spectral subtraction routine are 0.947%, 0.961%, and 3.55%, respectively, compared with 0.983%, 0.991%, and 3.57% of the feature from the blind deconvolution routine. The latter has better correlation with the crack growth curve than the former, whereas the precision is almost the same. From the comparison of the three defined performance indexes, it is clear that substantial feature improvements have been achieved via the application of the denoising algorithm. In the tables, "D.N" stands for denoised.

C. Performance on Failure Prognosis

A fault detection/failure prognosis framework based on particle filtering algorithms has successfully been developed and applied to the prediction of the RUL of the critical components [8], [13]. The approach provides a particle-filter-based estimate of the state probability density function (PDF), generates p-step-ahead long-term predictions, and uses available empirical information about hazard thresholds to estimate the RUL PDF. The algorithm implementation requires a process model to incorporate the information present in the feature data. Therefore, the following crack growth state model (based on the Paris equation) has been established for online state and model parameter estimation, as well as RUL PDF estimation:

$$\begin{cases} L(t+1) = L(t) + C\cdot\alpha(t)\cdot(\Delta K(t))^m + \omega_1(t) \\ \alpha(t+1) = \alpha(t) + \omega_2(t) \\ \Delta K(t) = f\left(\mathrm{Load}(t), L(t)\right) \end{cases}$$
$$\mathrm{Feature}(t) = h\left(L(t)\right) + v(t) \tag{16}$$

where $L(t)$ is the total crack length estimation at GAG cycle t contaminated by non-Gaussian white noise $\omega_1(t)$, $\alpha(t)$ is an unknown time-varying model parameter to be estimated contaminated by another non-Gaussian white noise $\omega_2(t)$, C and m are constants related to material properties, $\Delta K(t)$ is the variation in crack tip stress due to the load profile and the current crack length, f is a nonlinear function to map the load profile and the crack length to stress, and h estimates the crack length based on the value of feature, which is contaminated by non-Gaussian white noise $v(t)$. As a result, two loops are running in parallel in this algorithm: An inner loop updates the crack length and the RUL PDF estimate using the feature data and the previous state PDF estimates, whereas an outer loop updates the nonlinear mapping h every GAG cycle. This way, in long-term prediction, each particle generates a trajectory of the states. The statistical information of all these trajectories can be transferred into an RUL PDF at any given time instant. More details about this prognosis framework can be found in [8] and [13].

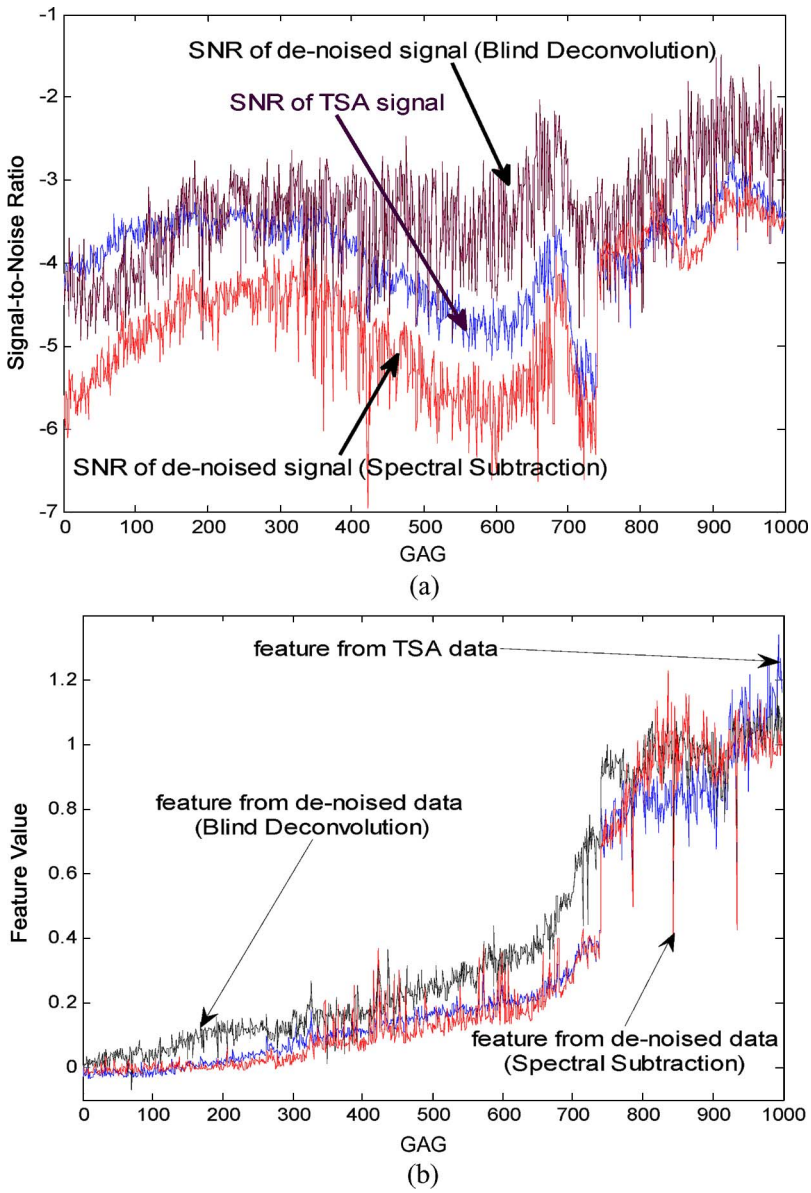

Fig. 6. SBR(12) before and after denoising. (a) SNR at 100% torque. (b) SBR(12) at 100% torque.

TABLE I
PERFORMANCE OF FEATURE SBR

Torque	20%		40%		100%	
	TSA	D.N	TSA	D.N	TSA	D.N
CCR	0.943	0.975	0.979	0.985	0.953	0.983
CCS	0.950	0.982	0.986	0.992	0.971	0.991
PMD	2.06%	2.01%	2.57%	2.73%	5.57%	3.57%

In this experiment, failure is defined when the crack reaches 6.21 in, i.e., the crack reaches the edge of the carrier plate. The ground truth data show that the crack reaches this value at the 714th GAG cycle. Therefore, the RUL PDF of the crack length at 6.21 in will be analyzed. In this section, results are shown to compare the algorithm performance when using the features derived in the previous section, before and after denoising. This will illustrate the efficiency of the proposed algorithm on the prediction of RUL in the helicopter testbed.

To evaluate the performance of the prognosis, statistics such as 95% confidence intervals (CIs) and RUL expectations are used. Since the gearbox operates based on GAG cycles, they are also given in units of "GAG cycle." Statistics such as 95% CI provide the accuracy of prognosis and therefore should be a range that contains the ground truth value of the GAG cycle, which is the 714th GAG cycle. Moreover, a small 95% CI is more accurate than a large 95% CI. On the other hand, the RUL expectation gives the precision of prognosis, and a value close to the 714th GAG cycle is more precise than a value far from it. It is important to note that, in real applications, an RUL expectation lower than the actual expectation is preferred since it only makes a conservative decision to schedule maintenance earlier. However, a higher value of RUL expectation in the prediction might postpone the timely maintenance and involve the risk of operating beyond safety, resulting in damage or loss of vehicle.

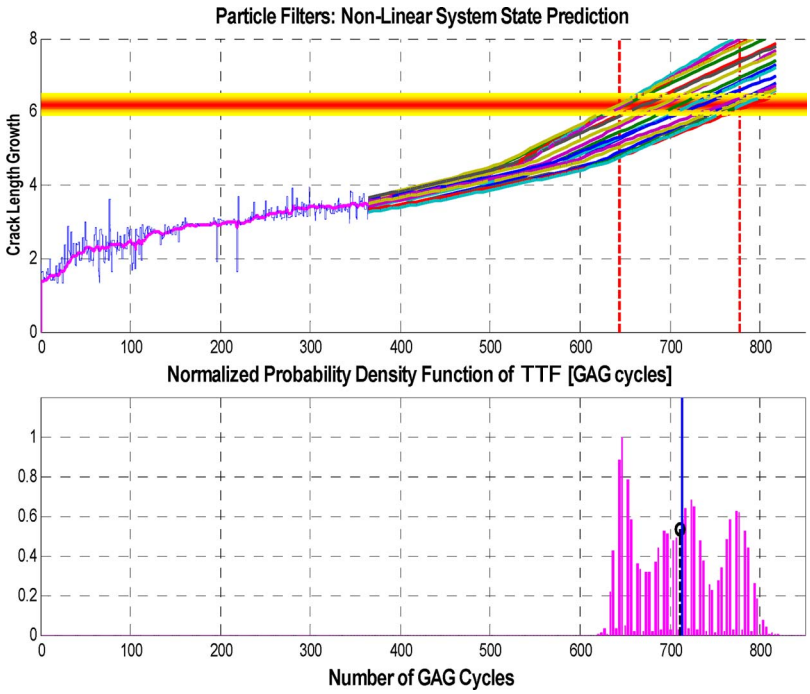

Fig. 7. Prognosis results from the 365th GAG cycle.

TABLE II
PERFORMANCE OF FAILURE PROGNOSIS

	Performance		Initial GAG cycle		
			365	400	450
Accuracy	TSA	95% CI	[637 773]	[663 832]	[680 828]
		CI Length	136	169	148
	D.N	95% CI	[638 777]	[647 775]	[618 720]
		CI Length	139	128	102
	CI Improvement TSA – (D.N)		**-3**	**41**	**46**
Precision	TSA	Expectation	705	747	754
	D.N	Expectation	710	711	670
	Improvement (714-TSA)/(714-DN)		**9/4**	**-34/3**	**-40/44**

In this experiment, at each GAG cycle, the current estimate of the state PDF is used as an initial condition. The result at the 365th GAG cycle from the denoised case is also shown in Fig. 7. More scenarios are summarized in Table II, where the accuracy CI improvement is the CI length with the TSA feature minus the CI length with denoised feature. The precision improvement is given as the ground truth value of 714 minus the expectation. Therefore, a positive value close to zero is preferred.

At the 365th GAG cycle, the accuracy and precision of two cases are very similar. At the 400th GAG cycle, both accuracy and precision have remarkable improvement. The CI length reduces 41 GAG cycles, which is about 125 min. As for the precision, the result based on the TSA feature gives an expectation of 747, which is beyond the 714th GAG cycle. If maintenance is scheduled based on this result, it will require the operation of the helicopter beyond its safety margin and risk the lives of the pilots. On the other hand, the results based on the denoised feature give a value very close to the 714th GAG cycle. At the 450th GAG cycle, the result is quite similar to the case at the 400th GAG cycle, except that the result of the denoised case is more conservative.

VI. CONCLUSION

The implementation of failure prognosis requires a high-quality feature to propagate the failure. Good features are often extracted from vibration signals, and noise might mask the signatures of the faults/failures. Therefore, preprocessing and denoising are important. This paper introduces the development of a new vibration signal blind deconvolution denoising scheme in synergy with feature extraction, failure prognosis, and vibration modeling to improve the SNR, the quality of the features, and the accuracy and precision of the failure prognostic algorithms. The proposed scheme is applied to the failure prognosis of a helicopter gearbox testbed for verification purposes.

REFERENCES

[1] G. Vachtsevanos, F. Lewis, M. Roemer, A. Hess, and B. Wu, *Intelligent Fault Diagnosis and Prognosis for Engineering Systems*. Hoboken, NJ: Wiley, 2006.

[2] B. Wu, A. Saxena, T. Khawaja, R. Patrick, G. Vachtsevanos, and R. Sparis, "An approach to fault diagnosis of helicopter planetary gears," in *Proc. IEEE AUTOTESTCON*, San Antonio, TX, Sep. 2004, pp. 475–481.

[3] M. Lebold, K. McClintic, R. Campbell, C. Byington, and K. Maynard, "Review of vibration analysis methods for gearbox diagnostics and prognostics," in *Proc. Soc. Mach. Failure Prevention Tech. 54th Meeting*, Virginia Beach, VA, May 2000, pp. 623–634.

[4] J. Keller and P. Grabill, "Vibration monitoring of UH-60A main transmission planetary carrier fault," in *Proc. Amer. Helicopter Soc. 59th Annu. Forum*, Phoenix, AZ, 2003, pp. 1–11.

[5] P. McFadden and J. Smith, "An explanation for the asymmetry of the modulation sidebands about the tooth meshing frequency in epicyclic gear vibration," in Proc. Inst. Mech. Eng. C, Mech. Eng. Sci., 1985, vol. 199, pp. 65–70.
[6] A. Szczepanik, "Time synchronous averaging of ball mill vibrations," *Mech. Syst. Signal Process.*, vol. 3, no. 1, pp. 99–107, Jan. 1989.
[7] R. Patrick, "A model-based framework for fault diagnosis and prognosis of dynamical system with an application to helicopter transmissions," Ph.D. dissertation, Georgia Inst. Technol., Atlanta, GA, May 2007.
[8] M. Orchard, "A particle filtering-based framework for on-line fault diagnosis and failure prognosis," Ph.D. dissertation, Georgia Inst. Technol., Atlanta, GA, Nov. 2007.
[9] J. Antoni, "Blind separation of vibration components: Principles and demonstrations," *Mech. Syst. Signal Process.*, vol. 19, no. 6, pp. 1166–1180, Nov. 2005.
[10] B. Klamecki, "Use of stochastic resonance for enhancement of low-level vibration signal components," *Mech. Syst. Signal Process.*, vol. 19, no. 2, pp. 223–237, Mar. 2005.
[11] J. Antoni and R. Randall, "Unsupervised noise cancellation for vibration signals: Part I—Evaluation of adaptive algorithms," *Mech. Syst. Signal Process.*, vol. 18, no. 1, pp. 89–101, Jan. 2004.
[12] D. Kundur and D. Hatzinakos, "A novel blind deconvolution scheme for image restoration using recursive filtering," *IEEE Trans. Signal Process.*, vol. 46, no. 2, pp. 375–390, Feb. 1998.
[13] M. Orchard, B. Wu, and G. Vachtsevanos, "A particle filter framework for failure prognosis," in *Proc. WTC III*, Washington, DC, Sep. 12–16, 2005.
[14] B. Zhang, T. Khawaja, R. Patrick, G. Vachtsevanos, M. Orchard, and A. Saxena, "Use of blind deconvolution de-noising scheme in failure prognosis," in *Proc. IEEE AUTOTESTCON*, Baltimore, MD, 2007, pp. 561–566.
[15] R. Patrick, M. Orchard, B. Zhang, G. Kacprzynski, M. Koelemay, and G. Vachtsevanos, "An integrated approach to helicopter planetary gear fault diagnosis and failure prognosis," in *Proc. IEEE AUTOTESTCON*, Baltimore, MD, 2007, pp. 547–552.
[16] S. Boll, "Suppression of acoustic noise in speech using spectral subtraction," *IEEE Trans. Acoust., Speech, Signal Process.*, vol. ASSP-27, no. 3, pp. 113–120, Apr. 1979.

Bin Zhang (SM'08) received the B.E. and M.S.E. degrees from Nanjing University of Science and Technology, Nanjing, China, in 1993 and 1999, respectively, and the Ph.D. degree from Nanyang Technological University, Singapore, in 2007.

Since 2005, he has been a Postdoctoral Researcher with the School of Electrical and Computer Engineering, Georgia Institute of Technology, Atlanta. His current research interests are fault diagnosis and failure prognosis, systems and control, digital signal processing, learning control, intelligent systems and their applications to robotics, power electronics, and various mechanical systems.

Taimoor Khawaja is currently working toward the Ph.D. degree with the School of Electrical and Computer Engineering, Georgia Institute of Technology (Georgia Tech), Atlanta.

He is currently investigating the blind deconvolution theory for designing efficient methods for signal denoising and exploring data-driven methods based on support vector machines and Bayesian inference for online fault detection and identification and failure prognosis at Georgia Tech. His research will contribute largely toward the autonomous monitoring of manufacturing systems and mission-critical equipment. His research interests include the design and implementation of real-time architectures for PHM systems.

Romano Patrick received the M.B.A. degree from Georgia Institute of Technology (Georgia Tech), Atlanta, the B.S. degree from the University of Panamericana, Mexico, the M.S. degree from the University of Texas, Arlington, and the Ph.D. degree in electrical and computer engineering, with specialization in model-based machine health diagnostics and prognostics, from Georgia Tech in 2007.

He is currently a Project Manager with Impact Technologies, Rochester, NY. His practice and academic studies focus on the interdisciplinary integration of hardware, software, and techniques to support cost-effective design and implementation of engineering systems. His past work and experience have involved electronic, mechanical, and software design; state-of-the-art process automation and novel machine health monitoring for a variety of industrial and government sponsors, including DARPA, Lockheed Martin, and Northrop Grumman; a three-year appointment as a Graduate Professor and Program Coordinator at the University of Panamericana; and some entrepreneurial R&D.

George Vachtsevanos (SM'89) received the B.E.E. degree from the City College of New York, New York, NY, in 1962, the M.E.E. degree from New York University, in 1963, and the Ph.D. degree in electrical engineering from the City University of New York in 1970.

He is a Professor Emeritus of electrical and computer engineering with the School of Electrical and Computer Engineering, Georgia Institute of Technology (Georgia Tech), Atlanta, where he directs the Intelligent Control Systems Laboratory, where faculty and students are conducting research on intelligent control, neurotechnology and cardiotechnology, fault diagnosis and prognosis of large-scale dynamical systems, and control technologies for unmanned aerial vehicles. His work is funded by government agencies and industry. He has authored more than 240 technical papers.

Dr. Vachtsevanos was a recipient of the 2002–2003 *Control Systems Magazine* Outstanding Paper Award (with L. Wills and B. Heck), the 2002–2003 Georgia Tech School of Electrical and Computer Engineering Distinguished Professor Award, and the 2003–2004 Georgia Tech Outstanding Interdisciplinary Activities Award.

Marcos E. Orchard received the B.Sc. degree and the Civil Industrial Engineering degree with Electrical Major from Catholic University of Chile, Santiago, Chile, in 1999 and 2001, respectively, and the M.S. and Ph.D. degrees from the Georgia Institute of Technology (Georgia Tech), Atlanta, in 2005 and 2007, respectively.

He is currently an Assistant Professor with the Department of Electrical Engineering, University of Chile. His current research interests include the design, implementation, and testing of real-time frameworks for fault diagnosis and failure prognosis.

Abhinav Saxena (M'08) received the B.Tech. degree in 2001 from the Indian Institute of Technology (IIT), Delhi, India, and the M.S. and Ph.D. degrees in electrical and computer engineering from the Georgia Institute of Technology, Atlanta.

He is a Staff Scientist with the Research Institute for Advanced Computer Science at the Prognostics Center of Excellence, NASA Ames Research Center, Moffett Field, CA. His research focus lies in developing prognostic algorithms for engineering systems and developing standard methods for evaluating performance of prognostic techniques.